Supporting Information

Oxidized Nanocarbons-Tripeptide Supramolecular Hydrogels: Shape Matters!

Daniel Iglesias[1], Manuel Melle-Franco[2], Marina Kurbasic[1], Michele Melchionna[1], Michela Abrami[3], Mario Grassi[3], Maurizio Prato[1,4,5], Silvia Marchesan[1].*

[a] Dipartimento di Scienze Chimiche e Farmaceutiche, Università di Trieste, Via Giorgieri 1, 34127 Trieste, Italy
[b] CICECO, University of Aveiro, 3810-193 Aveiro, Portugal
[c] Dipartimento di Ingegneria e Architettura, Università di Trieste, V. Valerio 6/1 - 34127 Trieste, Italy
[d] Carbon Nanobiotechnology Laboratory, CIC biomaGUNE, Paseo de Miramón 182, 20009 Donostia-San Sebastian, Spain
[e] Basque Fdn Sci, Ikerbasque, Bilbao 48013, Spain
* email: smarchesan@units.it

Table of Contents

1. Leu-^{D}Phe-^{D}Phe spectroscopic data

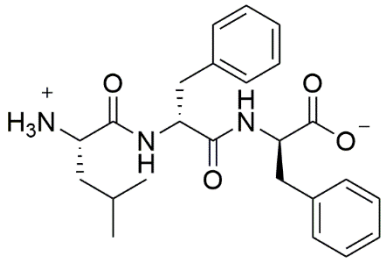

Fig. S1. Chemical structure of Leu-^{D}Phe-^{D}Phe in its zwitterionic form.

^{1}H NMR (500 MHz, DMSO-d_6) δ (ppm) 8.73 (d, J = 8.5 Hz, 1 H, NH), 8.62 (d, J = 8.6 Hz, 1 H, NH), 7.98 (broad s, 3 H, NH_3), 7.32 – 7.16 (m, 10 H, Ar), 4.72 (ddd, J = 10.6, 8.6, 4.5 Hz, 1 H, αCH), 4.47 (m, 1 H, αCH), 3.64 (m, 1 H, αCH), 3.11 (dd, J = 4.4 Hz, J_{gem} = 13.7 Hz, 1H, βCH_2), 2.95 (dd, J = 6.7 Hz, J_{gem} = 13.7 Hz, 1 H, βCH_2), 2.65 (dd, J = 7.8 Hz, J_{gem} = 13.7 Hz, 1 H, βCH_2), 2.78 (dd, J = 10.7 Hz, J_{gem} = 13.6 Hz, 1 H, βCH_2), 1.16 – 1.06 (m, 3 H, βCH, γCH_2), 0.68 (dd, J = 5.7 Hz, 6 H, δCH_3). **^{13}C NMR** (125 MHz, DMSO-d_6) δ (ppm) 172.7, 171.2, 168.7 (3 x CO); 137.5, 137.4, 129.3, 129.1, 128.3, 128.0, 126.5, 126.3 (Ar); 53.7, 53.6, 50.6 (3 x αC); 40.3, 38.1, 36.6 (3 x βC); 23.1, 22.5 (2 x γC); 21.7. (δC). **MS** (ESI): m/z 426.2 $[M+H]^+$ 448.2 $[M+Na]^+$ $C_{24}H_{31}N_3O_4$ requires 425.2.

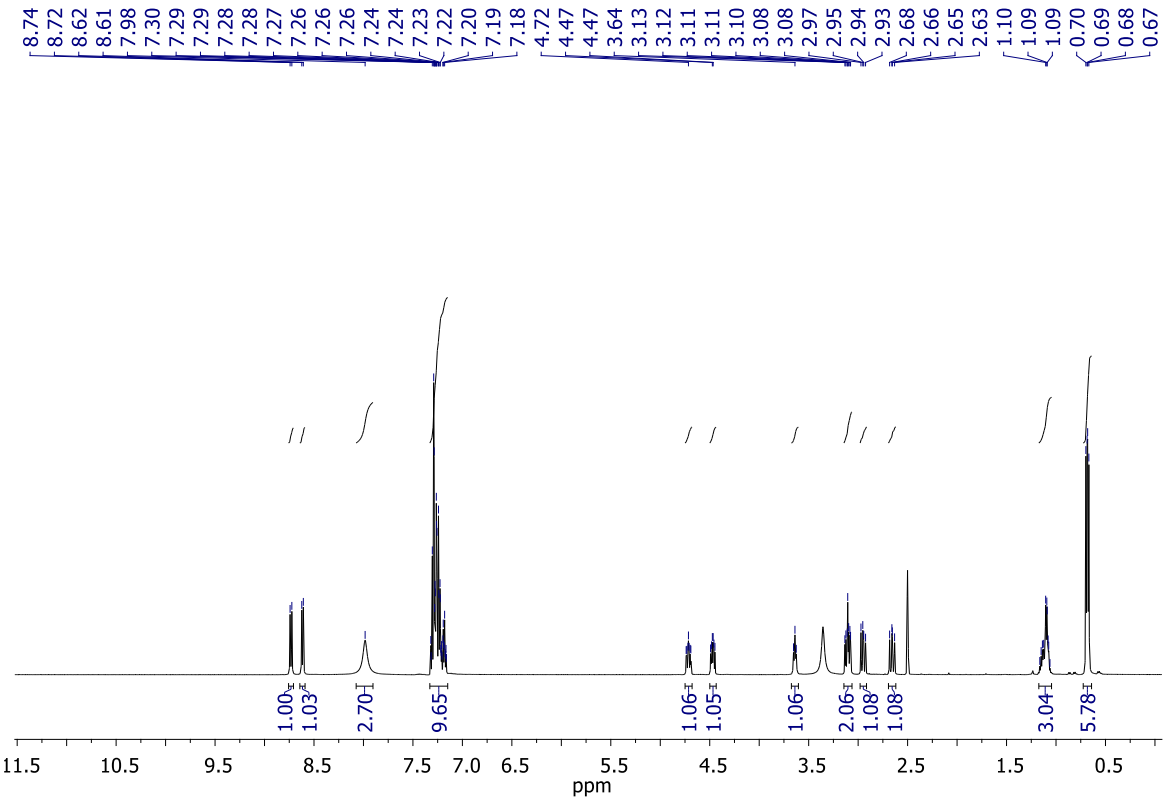

Fig. S2. ^{1}H-NMR spectrum of Leu-^{D}Phe-^{D}Phe.

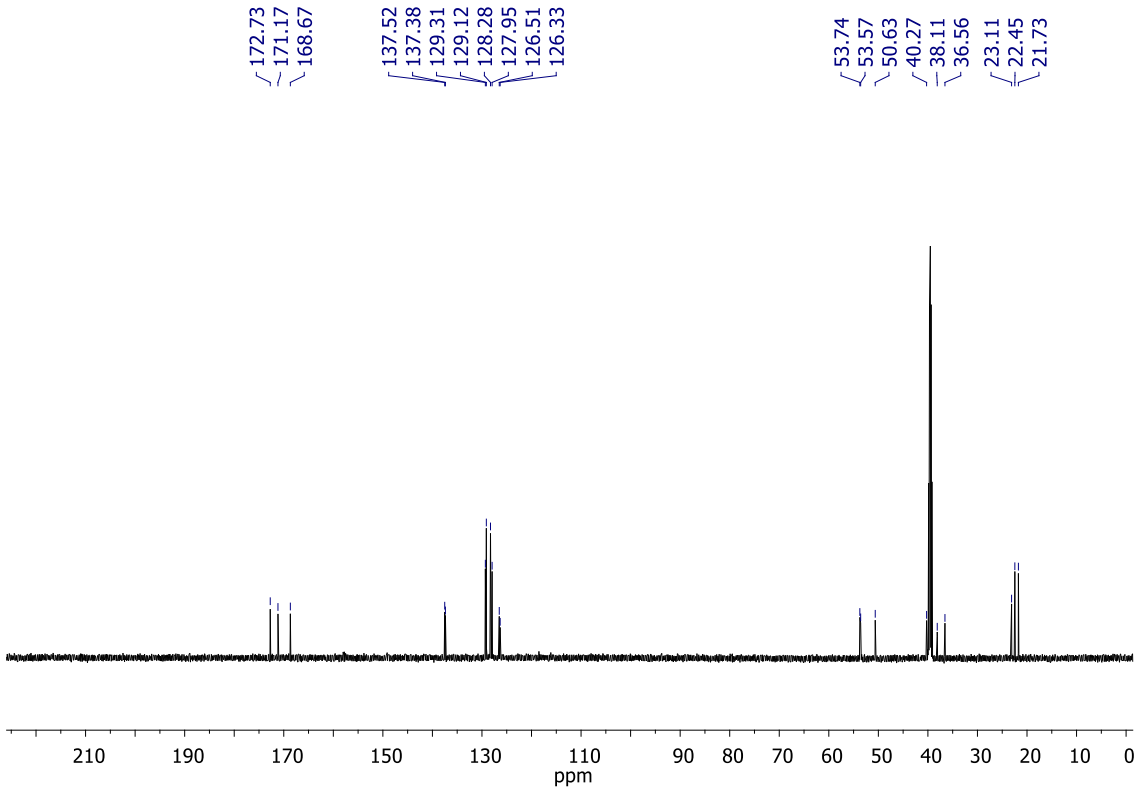

Fig. S3. ^{13}C-NMR spectrum of Leu-^{D}Phe-^{D}Phe.

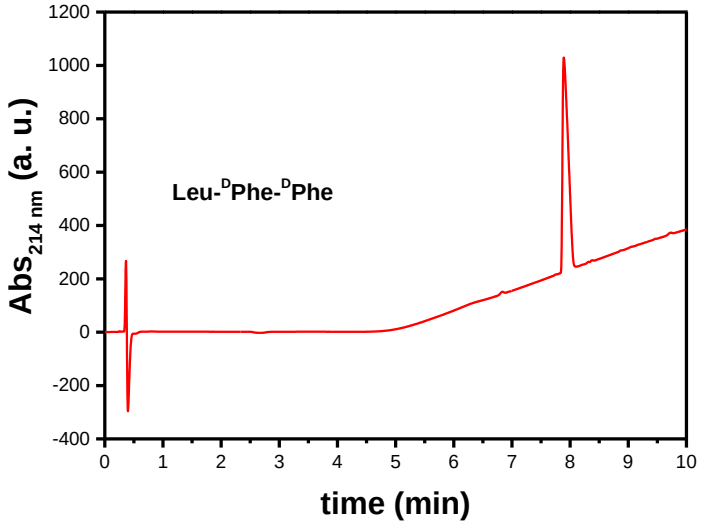

Fig. S4. LC-MS trace of Leu-^{D}Phe-^{D}Phe. Method: t = 0, 95% water (+0.1% HCOOH) and 5% MeCN (+0.1% HCOOH); t = 10 min, 5% water (+0.1% HCOOH) and 95 % MeCN (+0.1 % HCOOH). Flow 0.5 ml min^{-1}.

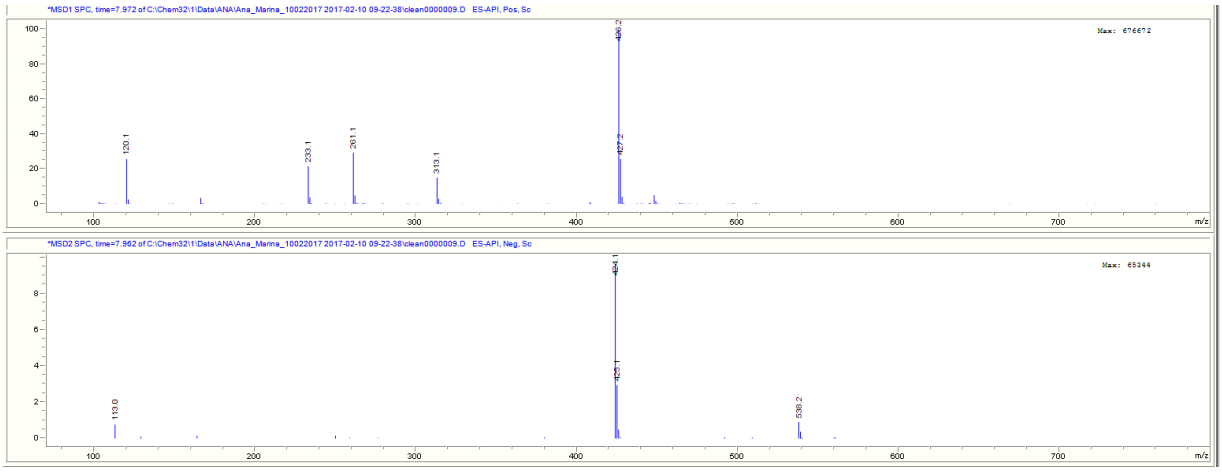

Fig. S5. ESI-MS spectra of Leu-^{D}Phe-^{D}Phe in positive (top) and negative (bottom) ion mode.

2. Rheological characterization of tripeptide hydrogels

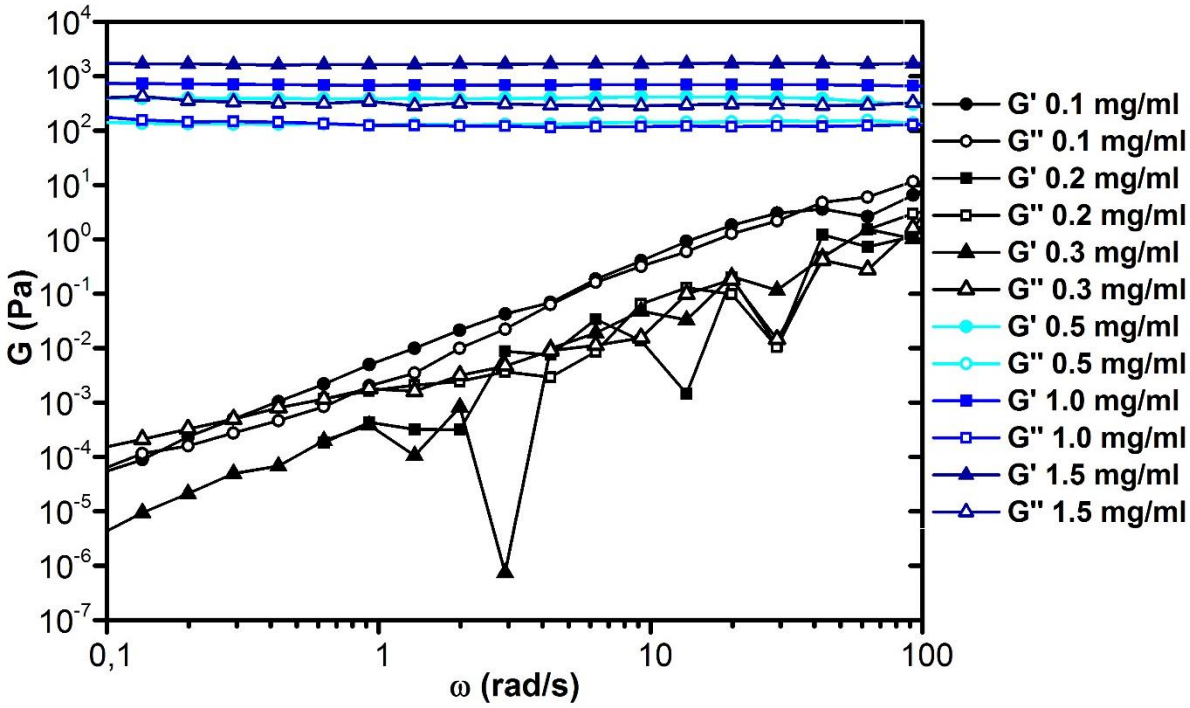

Fig. S6. Frequency sweep data at various concentrations of Leu-^{D}Phe-^{D}Phe tripeptide.

3. Characterization of oxidized nanocarbons

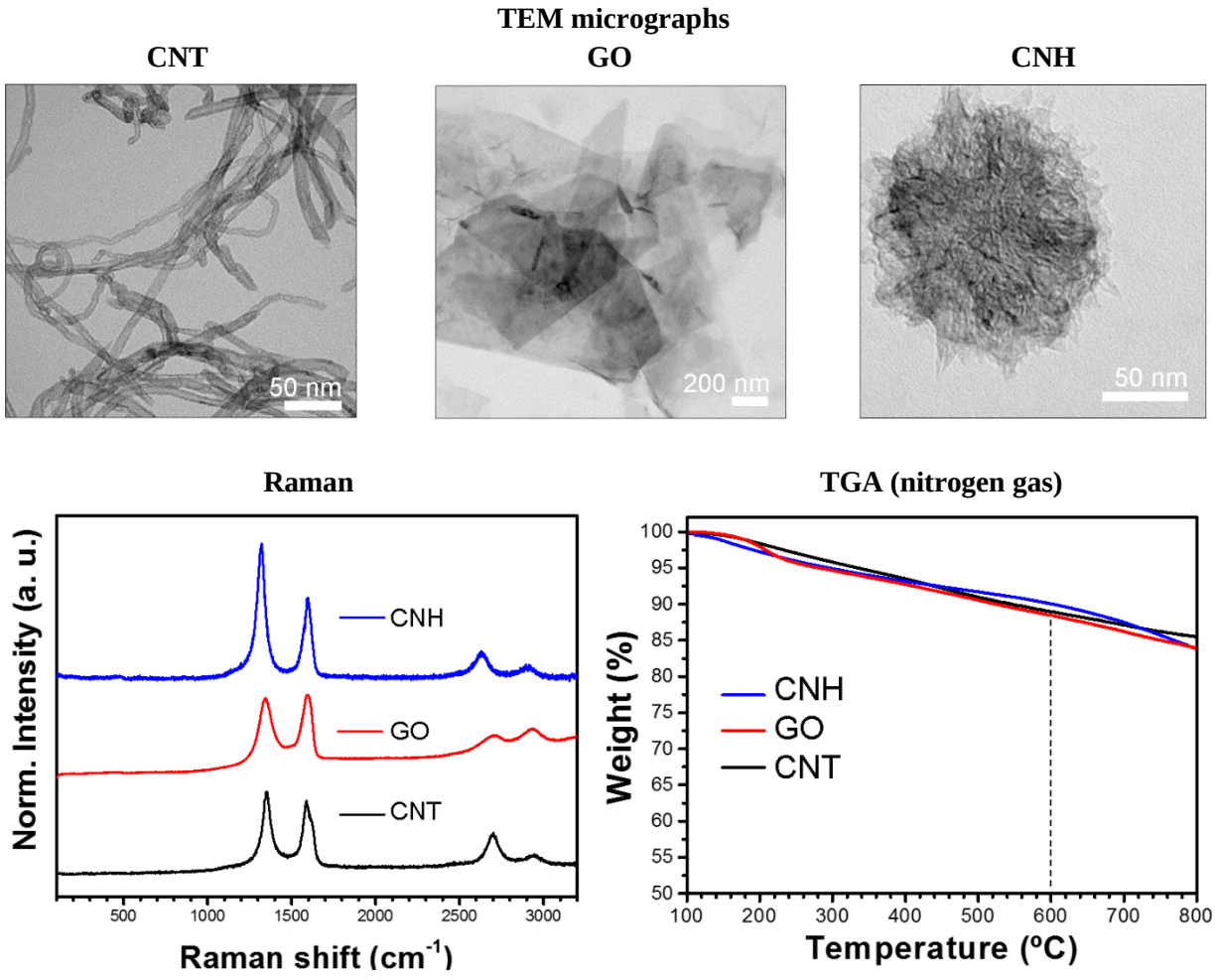

Fig. S7. Characterization data for oxidized nanocarbons.

4. Photographs of nanocarbon dispersions in the alkaline buffer

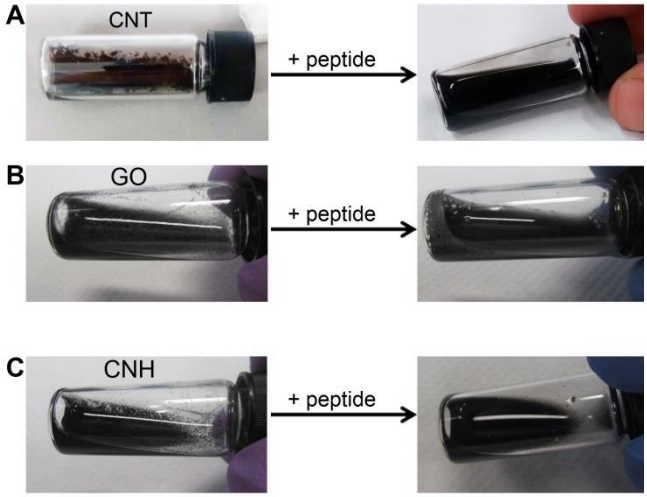

Fig. S8. Photographs of the nanocarbon dispersions in the alkaline buffer.

5. TEM images of peptide-nanocarbons at alkaline pH prior to self-assembly

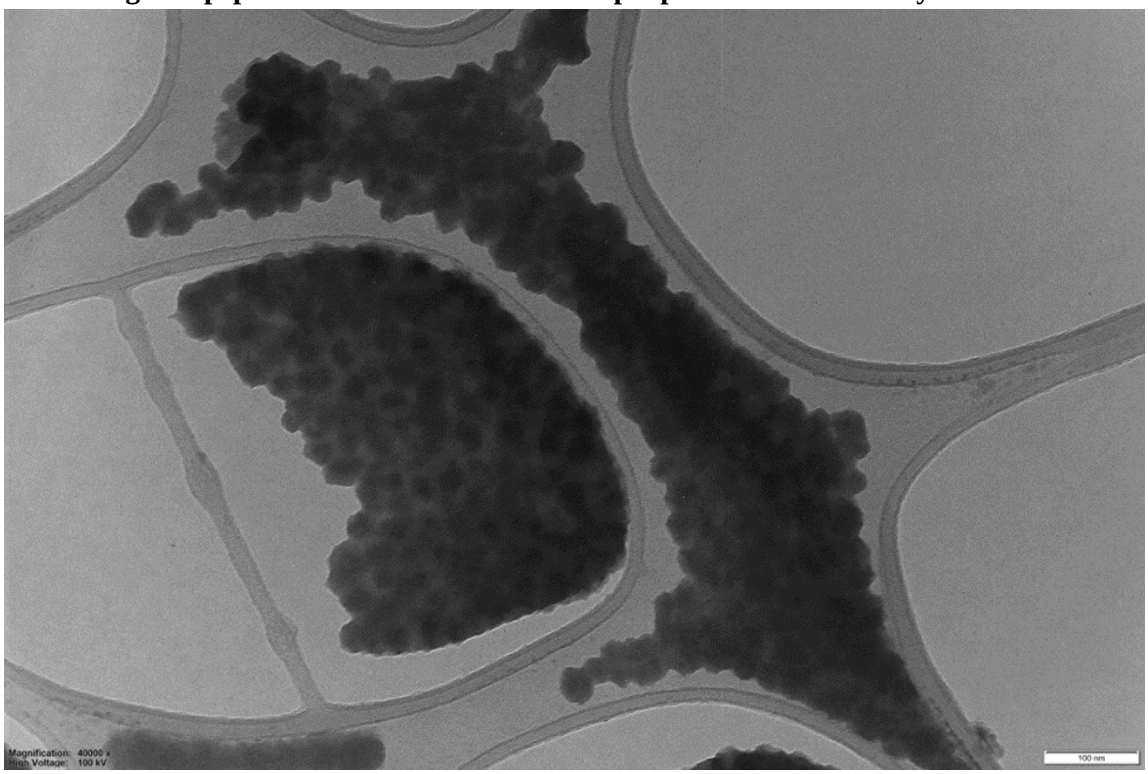

Fig. S9. TEM image of peptide in the alkaline buffer.

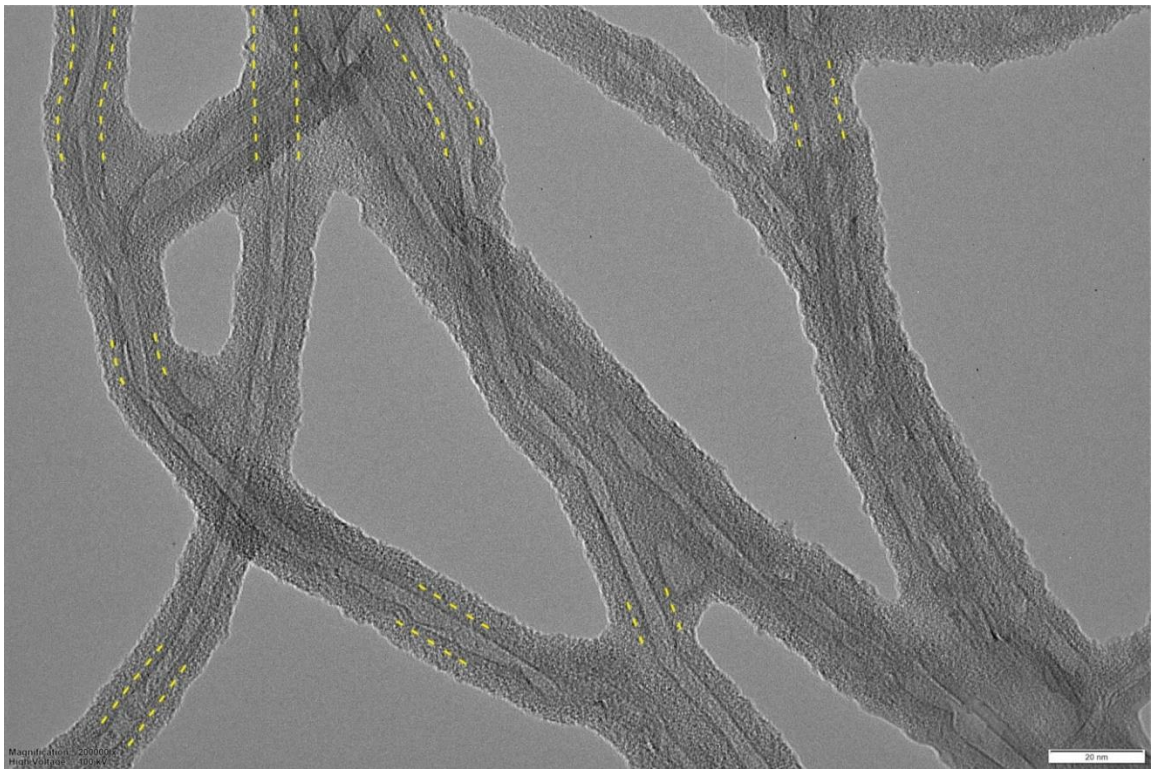

Fig. S10. TEM image of peptide-coated MWCNTs in the alkaline buffer. Dotted lines trace CNTs external wall to guide the eye.

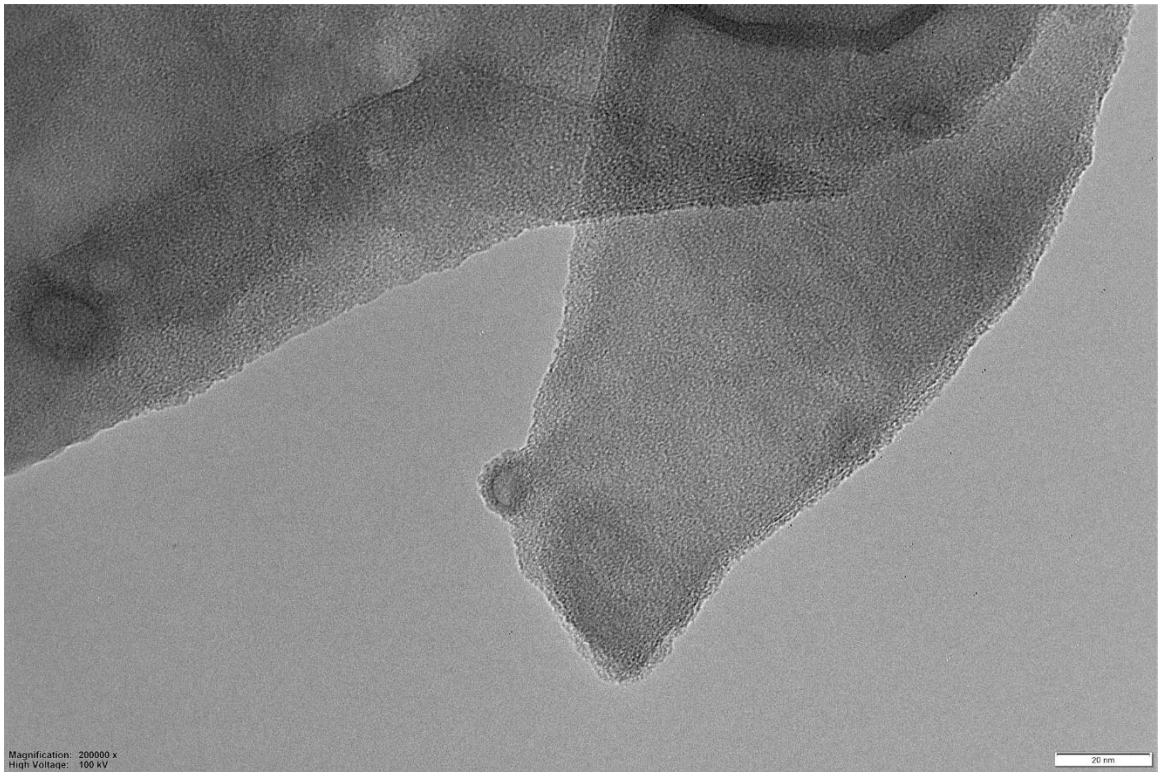

Fig. S11. TEM image of peptide-coated GO in the alkaline buffer.

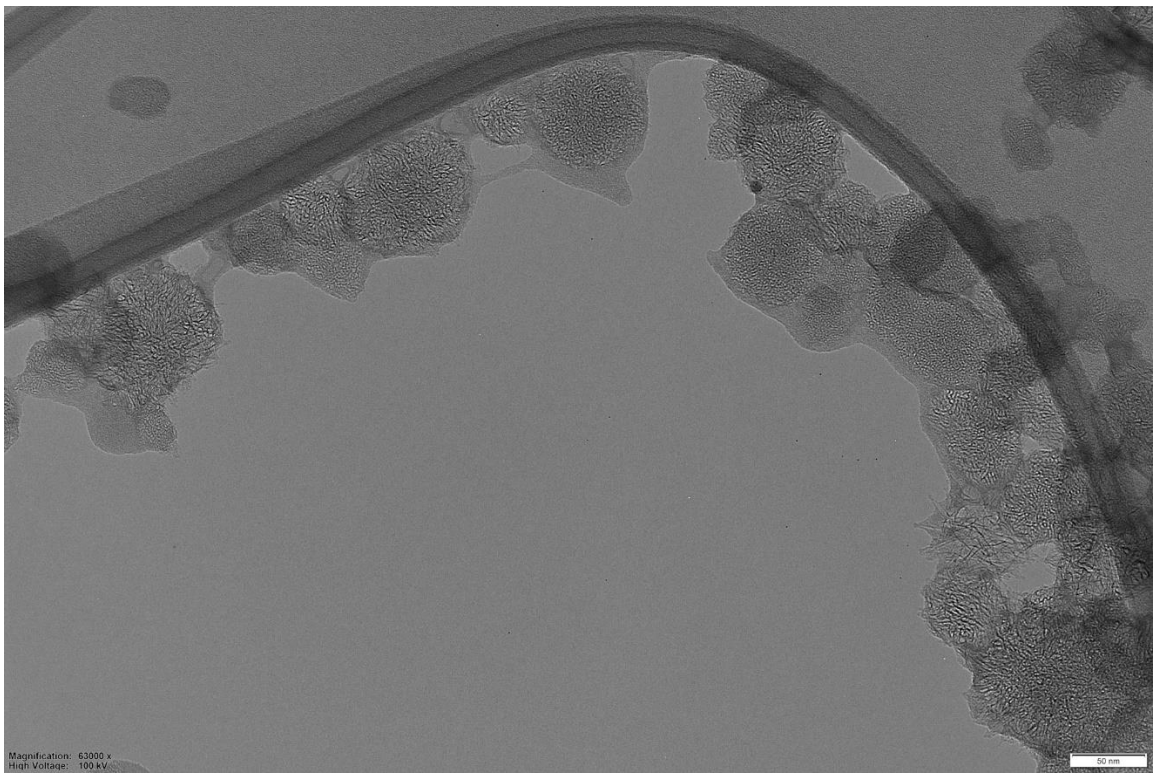

Fig. S12. TEM image of CNHs partially coated by peptide in the alkaline buffer.

6. AFM images of peptide-nanocarbons at alkaline pH prior to self-assembly

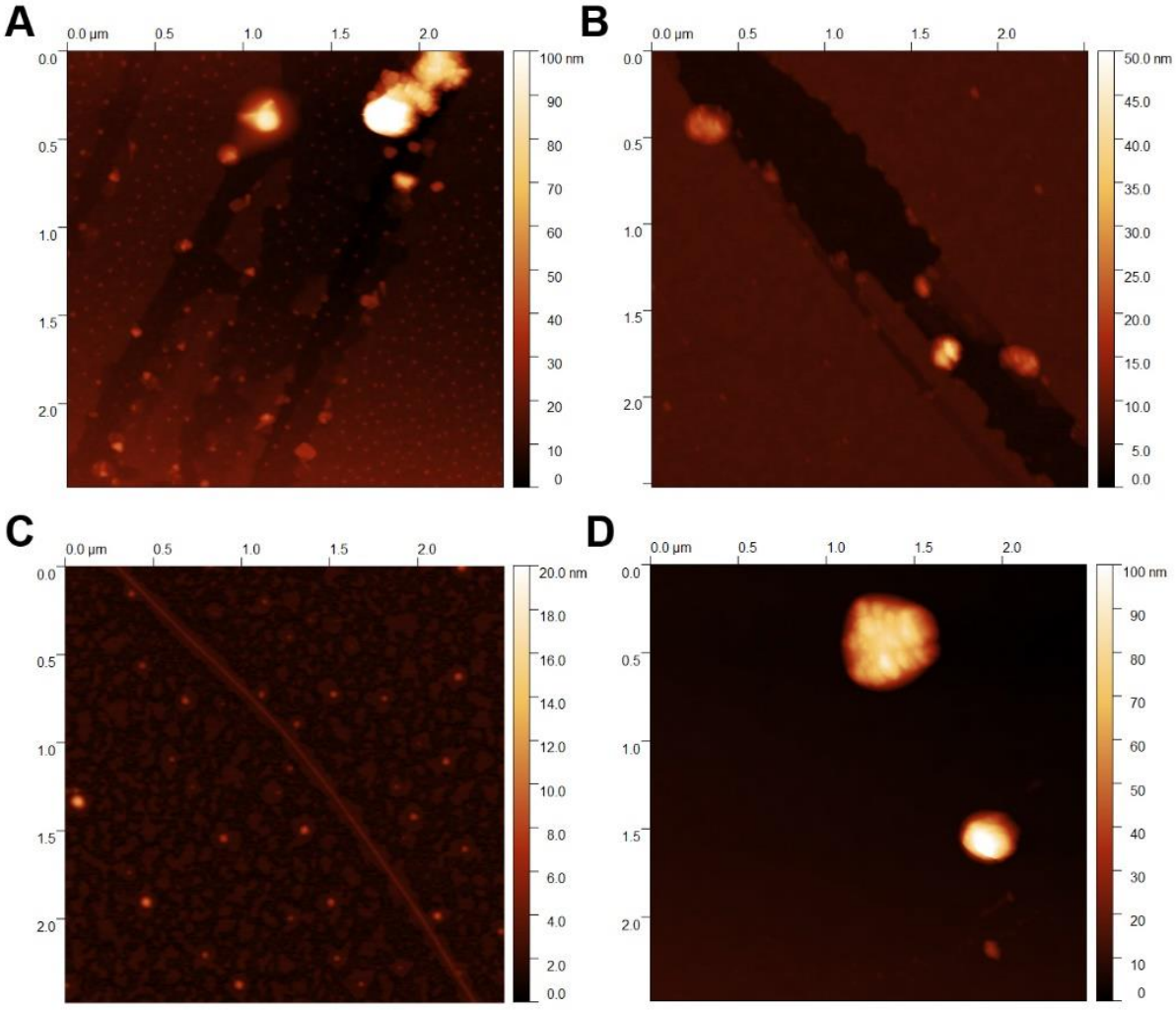

Fig. S13. AFM images of peptide alone (A), with GO (B), with CNTs (C), and with CNHs (D) in the alkaline buffer.

7. Peptide fibril and fiber diameter as calculated from TEM images.

Sample	Nanofibril diameter ± STD (nm)	Fiber diameter ± STD (nm)
Peptide alone	11.5 ± 2.2	44.2 ± 17.1
Peptide + CNT 1 mg/ml	12.2 ± 2.2	24.8 ± 6.2
Peptide + GO 1 mg/ml	10.2 ± 1.6	23.3 ± 4.6
Peptide + CNH 1mg/ml	10.9 ± 1.7	34.5 ± 8.3

Table S1. Average (n=100) diameter of peptide fibrils (after 1 h) and fibers (after 24 h) with or without nanocarbons.

8. Hydrogel mesh size evaluation

Flory's theory about gels enables the determination of the crosslink density ρ_x (defined as the moles of crosslinks between different polymeric chains per unit volume):

$$\rho_x = \frac{G}{RT}\left(\frac{\phi}{\phi_0}\right)^{\frac{2}{3}} \quad (1)$$

where G is the gel shear modulus, R is the universal gas constant, T is the absolute temperature while ϕ and ϕ_0 are, respectively, the gel polymer volume fraction in the swollen state and in the crosslinking state (in the case of this work, $\phi = \phi_0$ as gel did not undergo further swelling after its formation). G can be evaluated as the sum of all the spring constants of the generalized Maxwell model. This model assumes that the viscoelastic behaviour of every material can be properly described by a parallel disposition of n arms (elements) each one constituted by a spring (of constant G_i) and a dashpot (containing a fluid of viscosity η_i) in series. According to the generalised Maxwell model, the storage (or elastic, G') and the loss (or viscous, G'') moduli can be expressed by:

$$G' = G_e + \sum_{i=1}^{n} G_i \frac{(\lambda_i \omega)^2}{1+(\lambda_i \omega)^2}; \qquad G_i = \eta_i / \lambda_i \quad (2)$$

$$G'' = \sum_{i=1}^{n} G_i \frac{\omega\ \lambda_i}{1+(\lambda_i \omega)^2}; \quad (3)$$

where G_i and λ_i are, respectively, the spring constant and the relaxation time of the i^{th} element, ω is the solicitation pulsation ($= 2\pi f$, f = solicitation frequency) and G_e is the elastic constant of the first Maxell element that is supposed to purely elastic (its relaxation time goes to infinity). Eqs. (2)-(3) fitting to experimental frequency data (see, for example, Figure S6), according to a proper statistical procedure required to determine the number n of Maxwell elements, allows the determination of G_e and G_i. Thus $G = G_e + G_1 + G_2 + \ldots + G_n$.

Once ρ_x is known, the equivalent network theory of Schurz allows evaluating the average network mesh size ξ_a:

$$\xi_a = \sqrt[3]{6/\pi \rho_x N_A} \quad (4)$$

where N_A is the Avogadro number.

Sample	ξ - (nm)
Peptide hydrogel	16.1 ± 0.3
+ CNT	12.9 ± 0.3
+ GO	10.4 ± 0.1
+ CNH	12.3 ± 0.2

Table S2. Mesh size of hydrogel networks. ξ indicates the distance between two nodes of the network.

9. TEM images of peptide-nanocarbon hydrogels

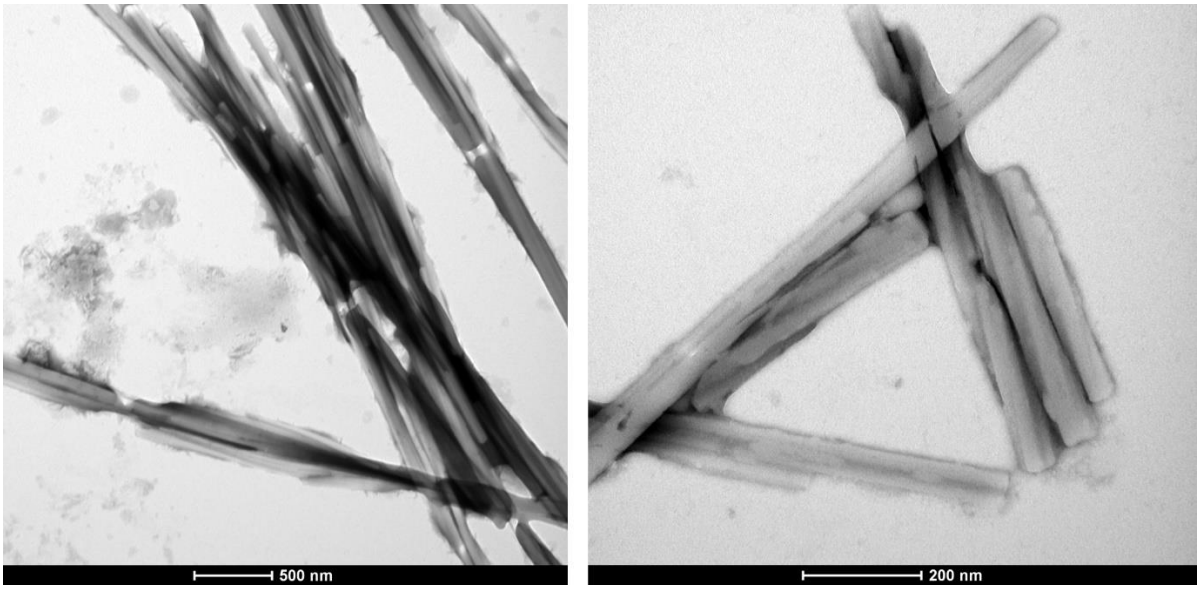

Figure S14. Peptide hydrogel.

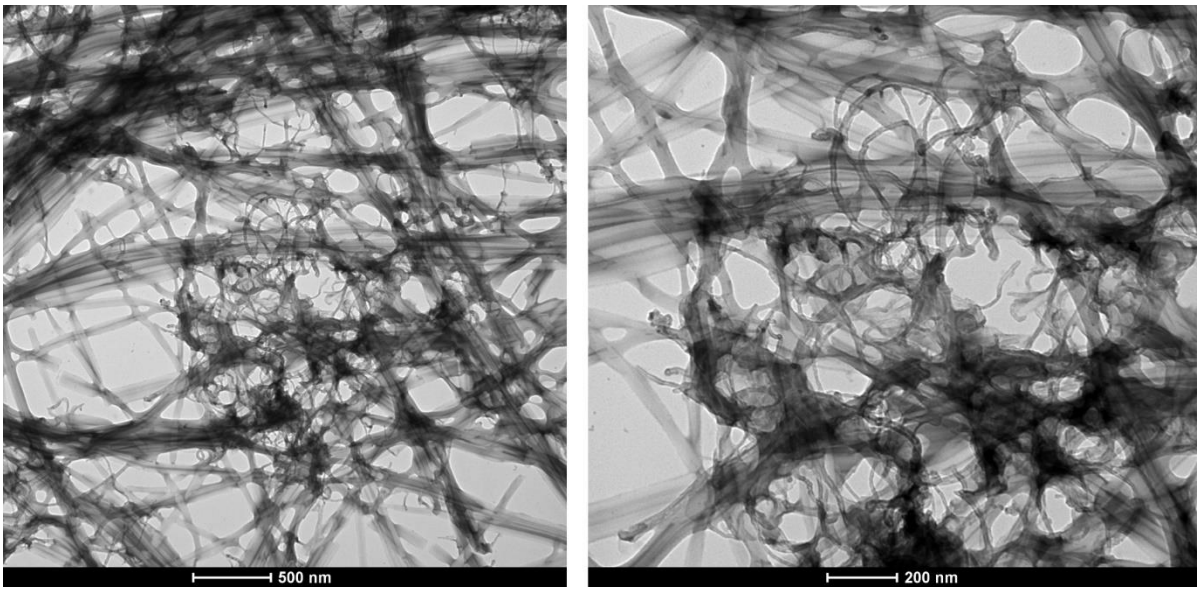

Figure S15. CNT-peptide hydrogel.

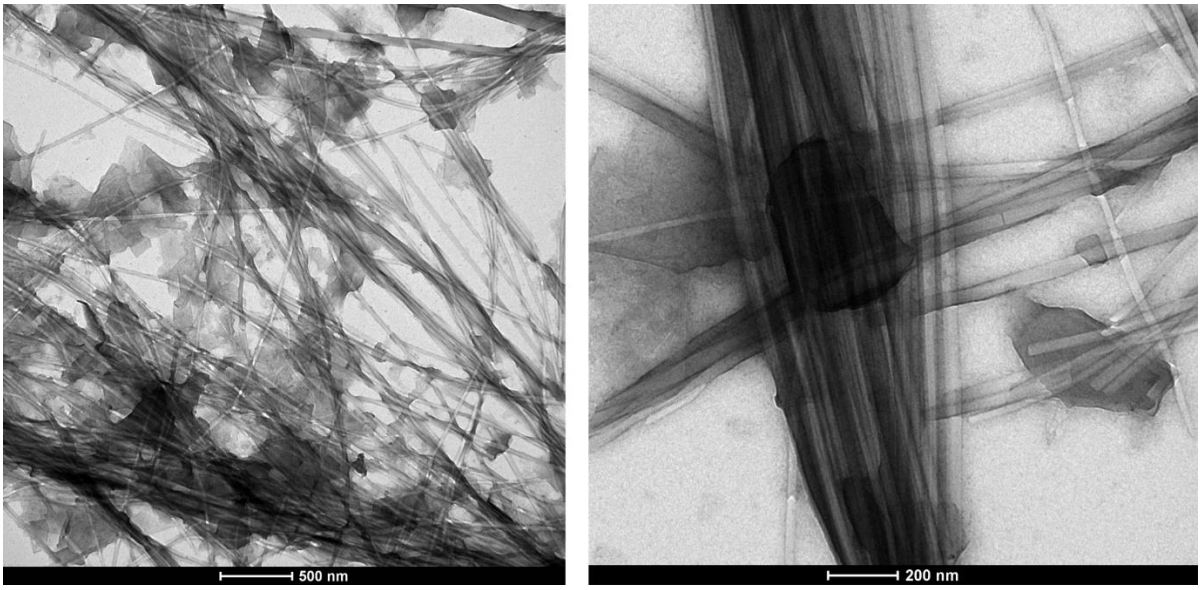

Figure S16. GO-peptide hydrogel.

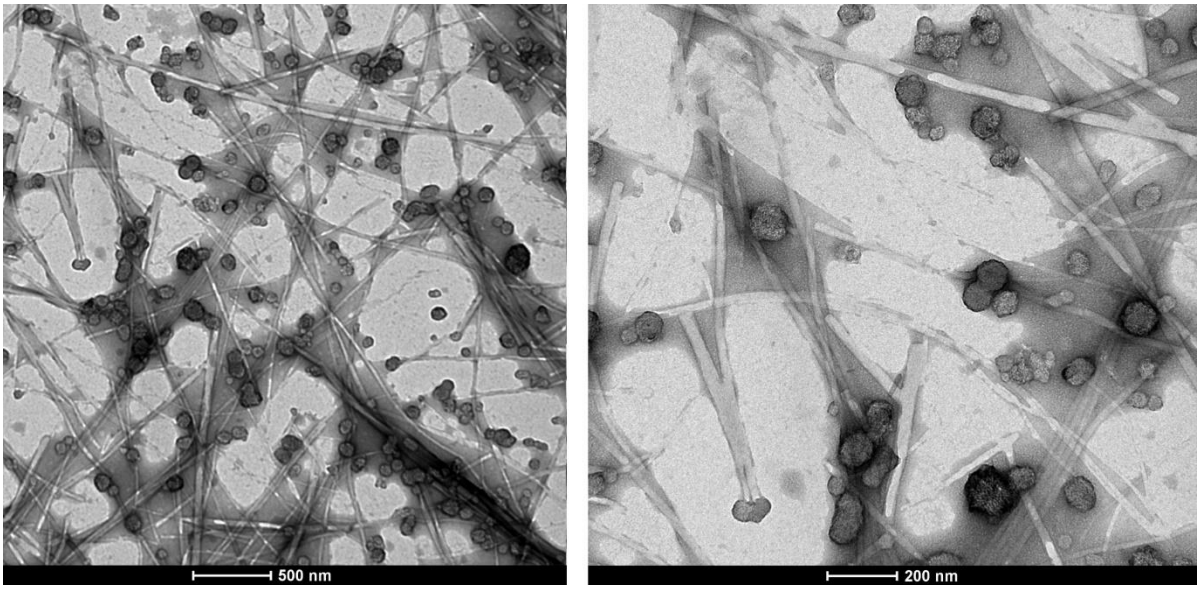

Figure S17. CNH-peptide hydrogel.

10. Rheological characterization of peptide-nanocarbon hydrogels

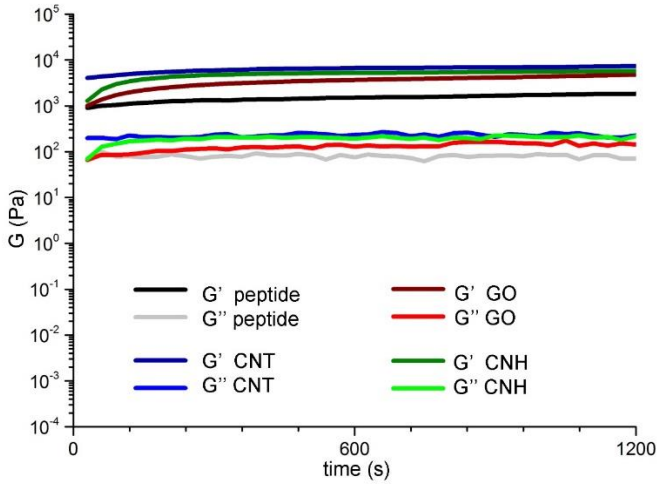

Fig. S18. Time sweep of peptide (black trace) and peptide-nanocarbon (colored traces) hydrogels.

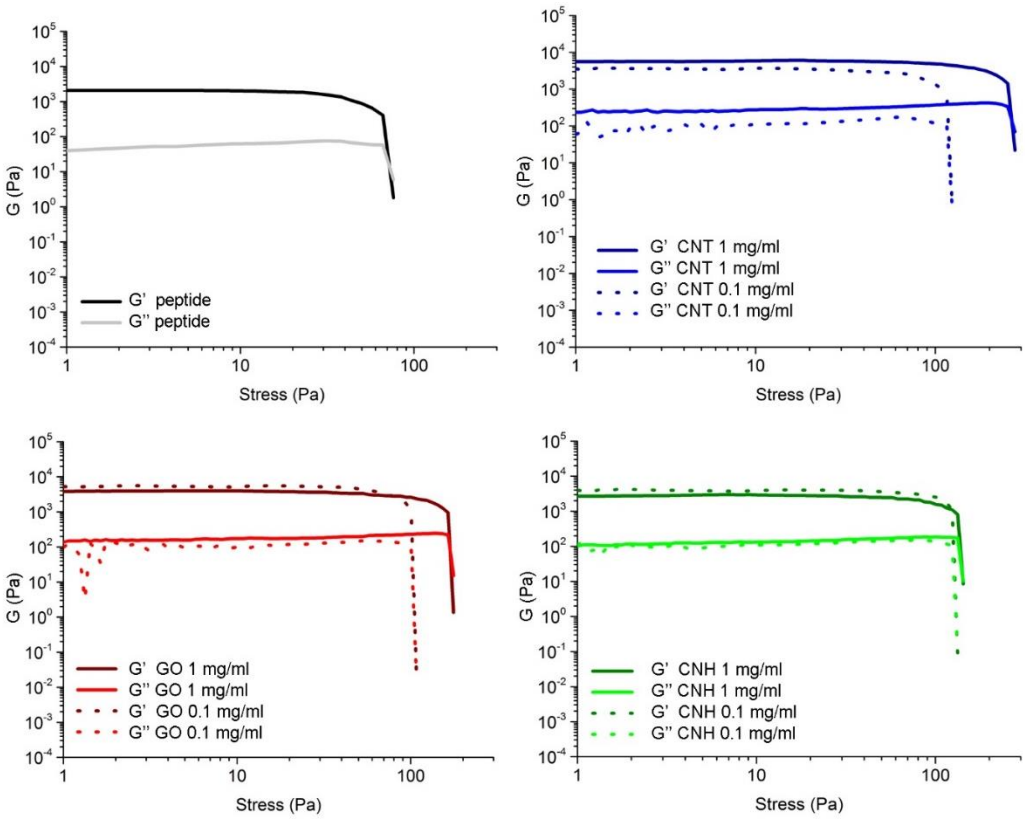

Fig. S19. Stress sweeps of peptide and peptide-nanocarbon hydrogels.

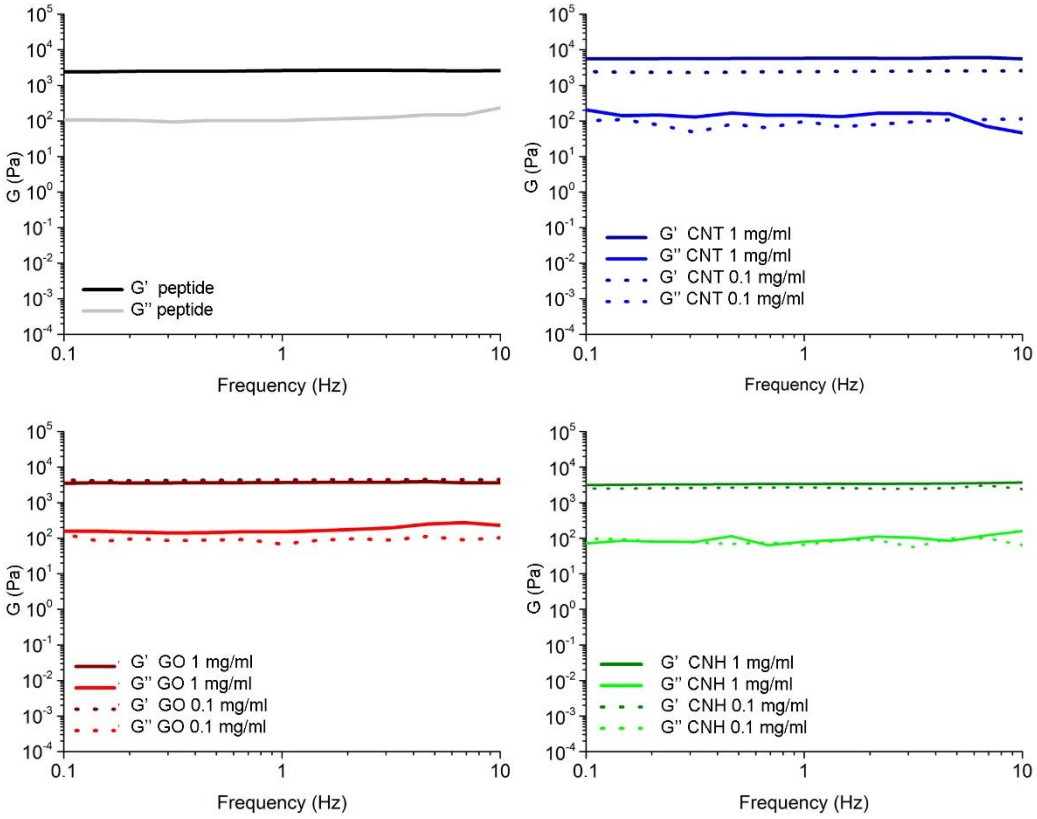

Fig. S20. Frequency sweeps of peptide and peptide-nanocarbon hydrogels.

Sample	G' ± STD (kPa)	G'' ± STD (kPa)
Peptide alone	2.0 ± 0.1	0.08 ± 0.02
Peptide + CNT 1 mg/ml	6.1 ± 2.0	0.20 ± 0.08
Peptide + GO 1 mg/ml	5.8 ± 1.0	0.20 ± 0.04
Peptide + CNH 1mg/ml	3.0 ± 0.3	0.15 ± 0.06

Table S3. Viscoelastic moduli of peptide-nanocarbon hydrogels (n=3).

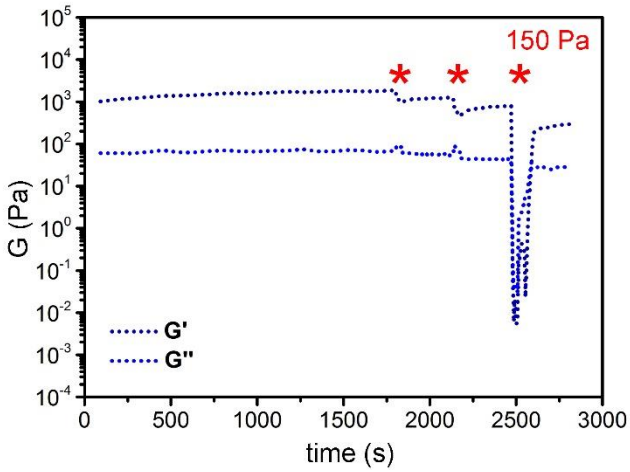

Fig. S21. Stress-recovery test for hydrogel with 0.1 mg ml^{-1} CNTs. After 30 min., the hydrogel is challenged with 30'' pulses at increasing stress (*i.e.*, 50, 100, and 150 Pa) with 5 min. intervals at 1 Pa to allow for recovery. The gel-to-sol transition occurs at 150 Pa, then the gel state is recovered.

11. AFM and TEM images of peptide-CNT fresh hydrogels

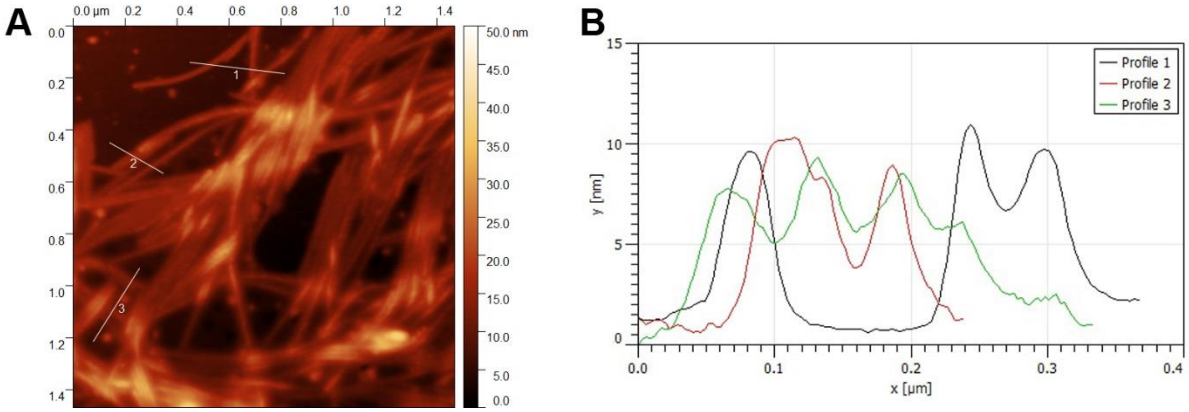

Fig. S22. AFM image of CNT-peptide hydrogel after 1 hour of self-assembly (left) and height linescans (right).

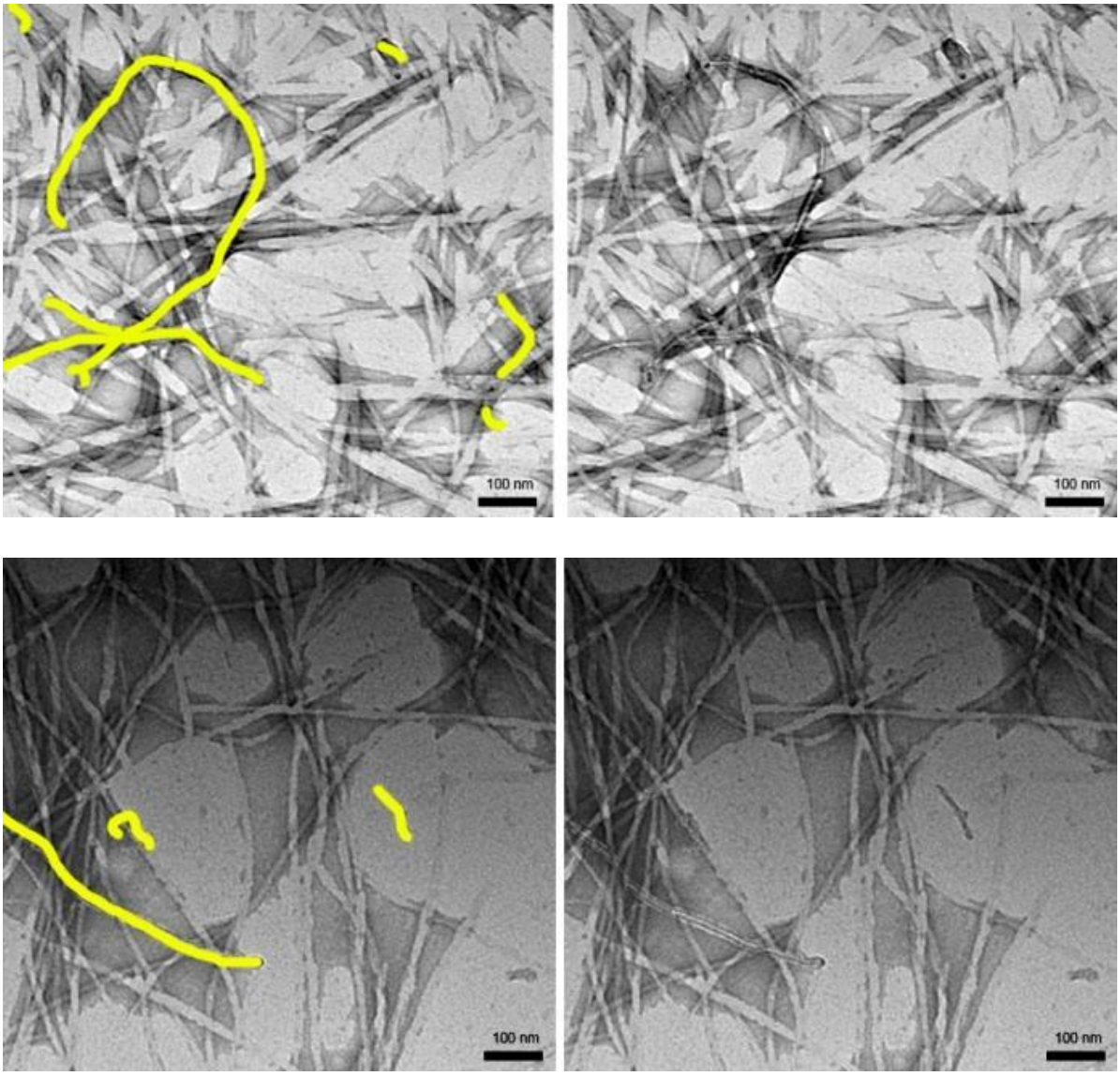

Fig. S23. TEM micrographs of peptide-CNT hydrogel fresh samples. Yellow lines trace CNTs.

12. Spectroscopic characterization of peptide-nanocarbon systems

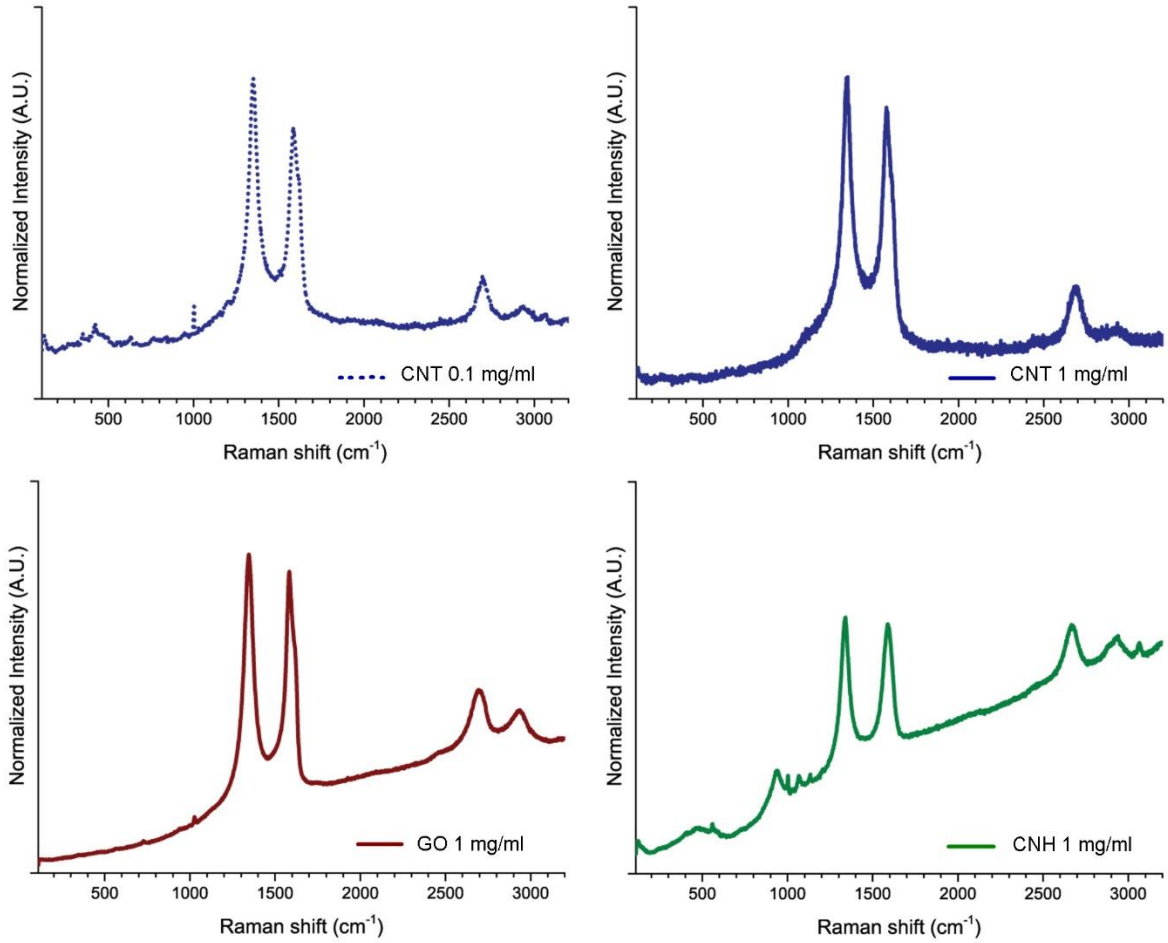

Fig. S24. Raman spectra of peptide-nanocarbon hydrogels.

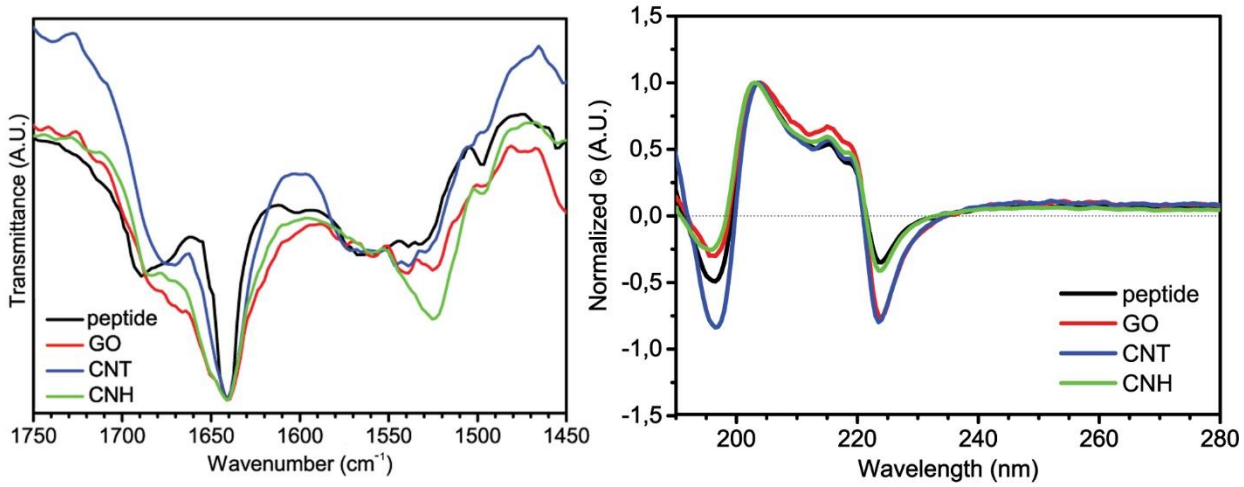

Fig. S25. ATR-IR (left) CD (right) spectra of peptide-nanocarbon gels. *Note:* CD signal intensity displayed high variability due to light scattering in the presence of nanocarbon.

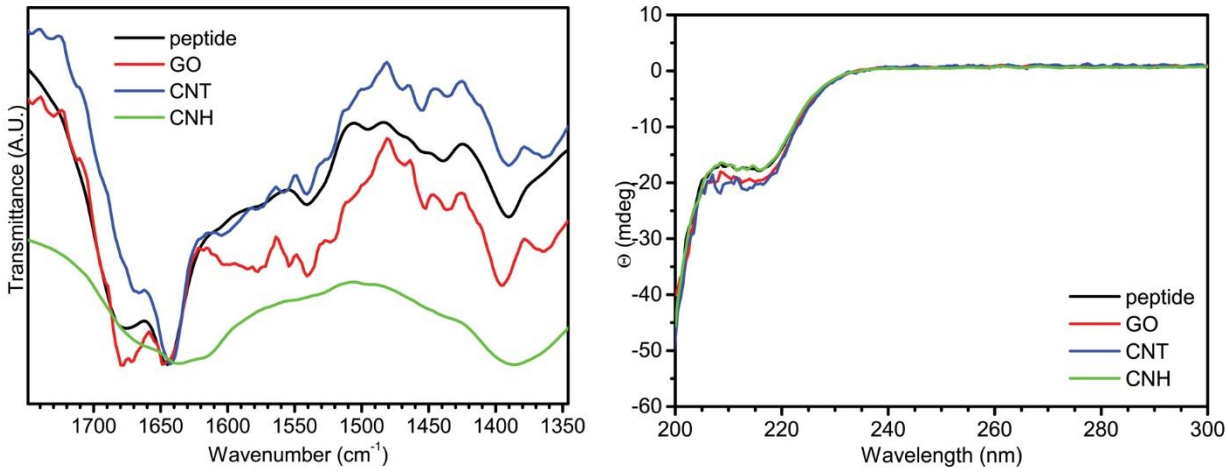

Fig. S26. ATR-IR (left) CD (right) spectra of peptide-nanocarbon gel precursor solutions.

13. *In silico* study of peptide-CNT system

Five systems were calculated varying the CNT model:

a. pristine CNT
b. 1% oxidized system, with 1% atoms on the external CNT surface with epoxide functionalization
c. 1% oxidized system, with 1% atoms on the CNT external surface with OH functionalization
d. 10% oxidized system, with 10% atoms on the external CNT surface with epoxide functionalization
e. 10% oxidized system, with 10% atoms on the CNT external surface with OH functionalization

The oxidized groups were randomly located on the external CNT. The epoxide and alcohol functionalized groups share the same locations at the same oxidation degrees. Both epoxide and alcohol models led to similar results, of which the alcohol is shown in the main MS. The tripeptide is considered in zwitterionic form, the terminal charged beads are represented as red (negative) and blue (positive) spheres. The unfunctionalized CNT beads are rendered as grey spheres while the functionalized beads are rendered as green spheres.

After 20M MD steps (shown in the main MS and in Fig. S16), the peptide-CNT systems are not fully equilibrated. Four periodic boxes in the direction perpendicular to the tube axis are represented in Fig. 6 in the MS and Fig. S16. For the pristine CNT (Fig. S16a), after 20M MD steps, most tripeptides have been adsorbed on the CNT. For the 1 % oxidation and epoxide functionalization there is a large sphere-like peptide agglomerate dispersed in water, and very little peptide is adsorbed onto the CNT (Fig. S16b). For the alcohol, more polar, functionalization, a similar pictures is observed but the aggregate is smaller and more adsorption is observed on the CNT (Fig. S16c). The 10 % oxidation shows a peptide fibre connecting the neighbouring CNTs spanning a 8.5 nm distance (Figs. S16d and S16e).

If we consider 10x longer simulation times, namely **200M MD steps (nominal simulation time 6 microseconds)**, the systems equilibrate to all tripeptides adsorbed onto a single CNT on approximately two adlayers (Fig. S17). Interestingly, all systems yield similar, full coverage of the CNT, although the 10% oxidized model with alcohol groups shows an empty region throughout the MD simulation.

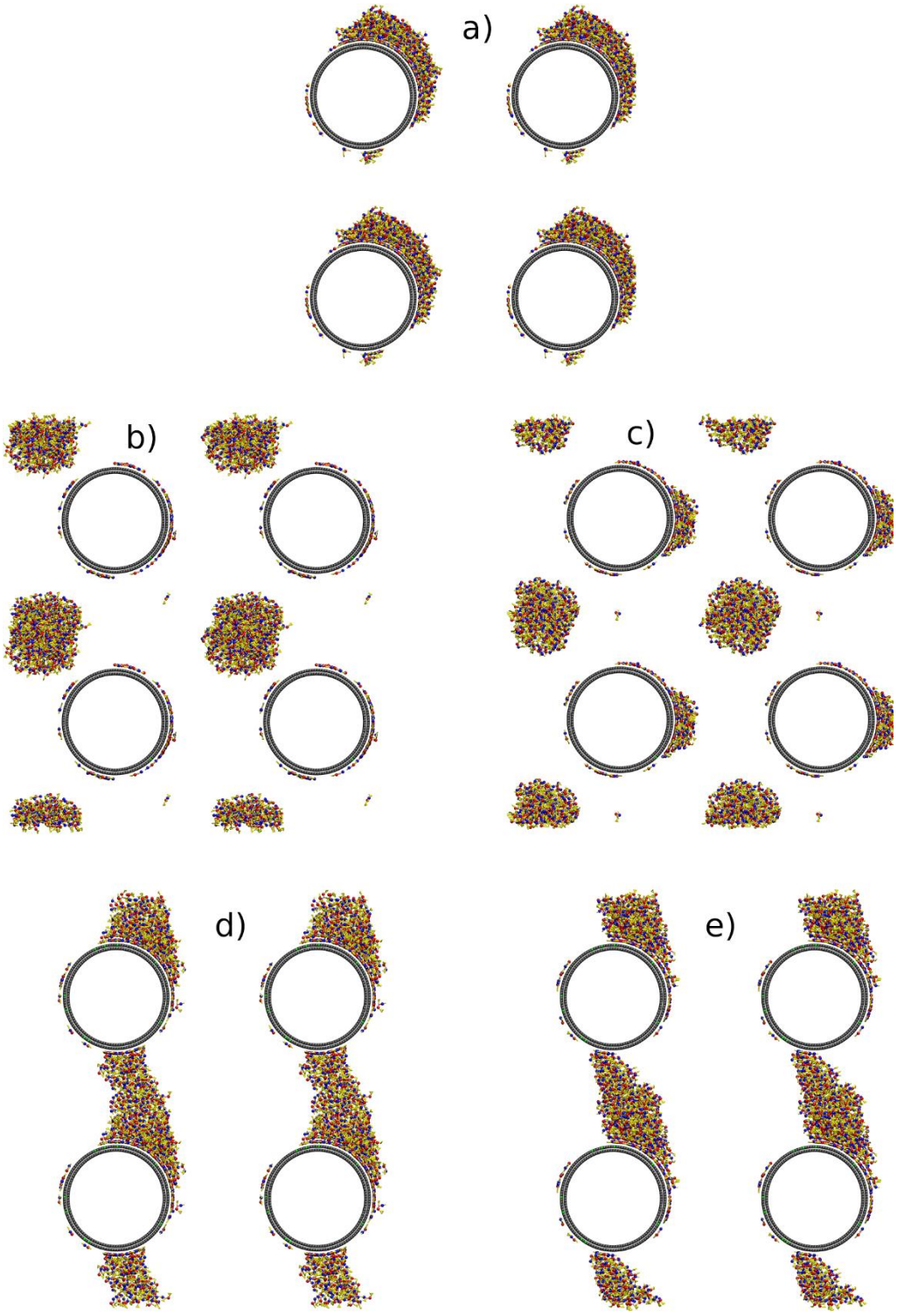

Fig. S27. Models of peptide-CNT systems after 20M MD steps. (a) Pristine CNT; 1 % oxidized CNT with (b) epoxide groups or (c) alcohol groups; 10 % oxidized CNT with (d) epoxide groups or (e) alcohol groups (c). The tripeptide is in zwitterionic form, the terminal charged beads are represented as red (negative) and blue (positive) spheres. The phenyl groups are modelled by three beads and are rendered as yellow triangles. The unfunctionalized CNT beads are represented as grey spheres while the functionalized beads are rendered as green spheres. Four periodic boxes in the direction perpendicular to the tube axis are represented.

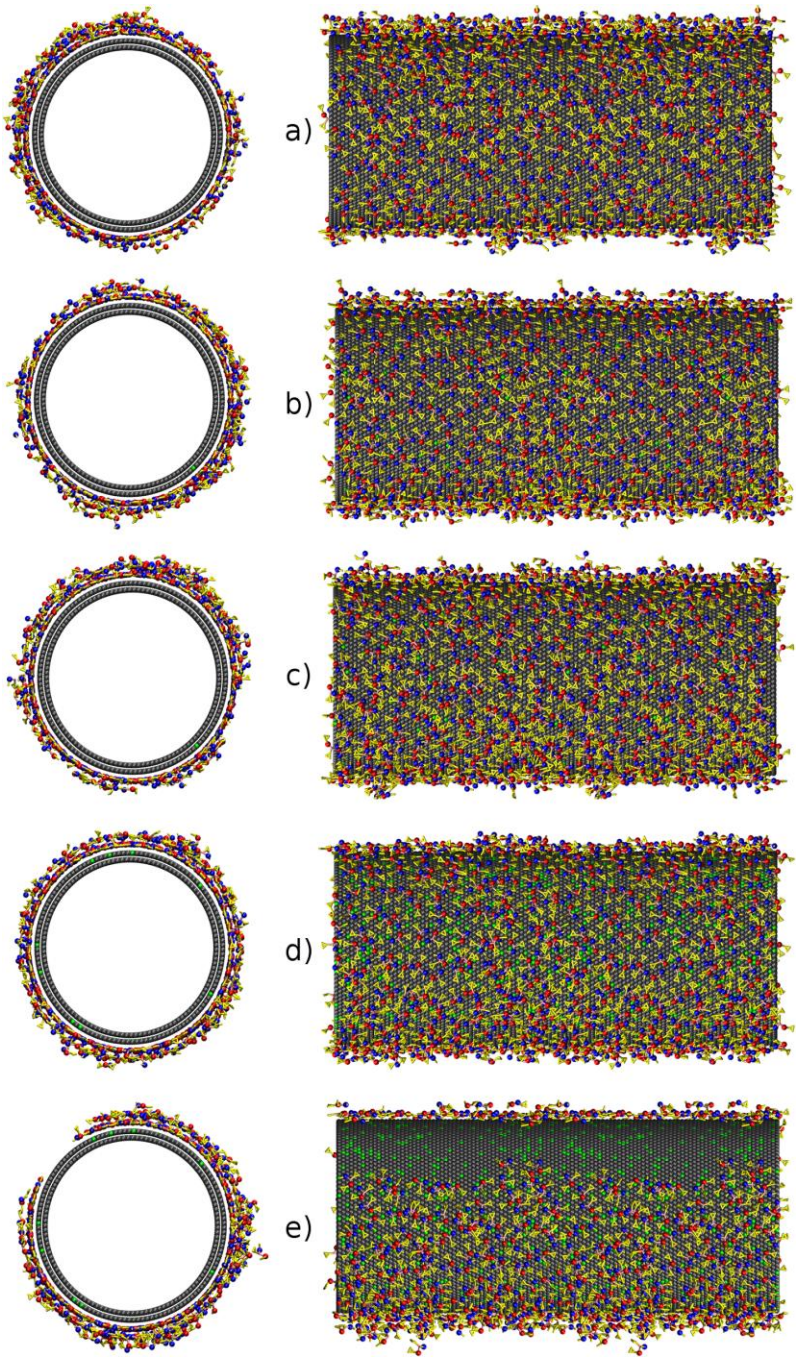

Fig. S28. Models of peptide-CNT systems after 200M MD steps. (a) Pristine CNT; 1 % w/w oxidized CNT with (b) epoxide groups or (c) alcohol groups; 10 % w/w oxidized CNT with (d) epoxide groups or (e) alcohol groups (c). The tripeptide is in zwitterionic form, the terminal charged beads are represented as red (negative) and blue (positive) spheres. The phenyl groups are modelled by three beads and are rendered as yellow triangles. The unfunctionalized CNT beads are represented as grey spheres while the functionalized beads are rendered as green spheres. Two periodic boxes in the direction parallel to the tube axis are represented.